

Ambient catalyst-free nitrogen fixation with water dimer radical cation

Xiaoping Zhang¹, Liping Huang², Jingling Li¹, Wenwen Yang¹, Konstantin Chingin², Roman Balabin², Jingjing Wang², Xinglei Zhang¹, Weifeng Zhu², Rui Su³, Keke Huang³, Shouhua Feng³, Huanwen Chen^{1,2*}

¹Jiangxi Key Laboratory for Mass Spectrometry and Instrumentation, East China University of Technology, Nanchang, 330013, P. R. China.

²School of Pharmacy, Jiangxi University of Chinese Medicine, Nanchang, 330004, P. R. China

³State Key Laboratory of Inorganic Synthesis and Preparative Chemistry, College of Chemistry, Jilin University, Changchun 130012, P. R. China

***Corresponding author.**

Prof. Dr. Huanwen Chen

Email: chw8868@gmail.com

Tel: (+86)791-8389-6370

Fax: (+86)791-8389-6370

1688 Meiling Road, Xinjian District, Nanchang, Jiangxi Province 330004 P. R. China

Abstract:

The growth and sustainable development of humanity is heavily dependent upon the process of fixing nitrogen (N_2) to ammonia (NH_3). However, the currently adopted methods are associated with severe environmental hazards and tremendous energy costs, which limit their sustainability and profitability. Herein we discovered a catalyst-free disproportionation reaction of N_2 by water dimer radical cation, $(\text{H}_2\text{O})_2^{+\bullet}$, which occurs under mild ambient conditions *via* distinctive $\text{HONH-HNOH}^{+\bullet}$ intermediate to yield economically valuable nitroxyl (HNO) and hydroxylamine (NH_2OH) products, in alternative to NH_3 . Calculations suggest that the reaction is prompted by the coordination of electronically excited N_2 with $(\text{H}_2\text{O})_2^{+\bullet}$ in its two-center-three-electron (2c-3e) configuration. Subsequent excited-state double proton transfer leads to one-step water addition to N_2 . The ambient fixation of N_2 into HNO and NH_2OH with high selectivity offers great profitability and total avoidance of polluting emissions, such as CO_2 or NO_y , thus giving an entirely new look and perspectives to the problem of green N_2 fixation.

Nitrogen is an essential element for all living organisms on our planet. Molecular nitrogen (N_2) accounts for more than 99% of global nitrogen ¹ but is extremely chemically stable and thus cannot be directly utilized unless fixed by alternating its oxidation state into bioavailable forms ². Since the advent of energy-intensive Haber-Bosch (HB) process early in the 20th century and up to the present time, N_2 on Earth has been predominantly fixed in the form of ammonia (NH_3), which has largely shaped our world and its heavy dependence on NH_3 ³. However, the intensive reaction conditions (ca. 100 bar and 500°C), severe environmental pollution (>1% of the global carbon emission) and high consumption of fossil fuel (1%–2% of global energy consumption) in the HB process are becoming increasingly crucial for the global sustainable development and urge novel strategies for N_2 fixation under mild conditions ^{4,5}. Extensive research is being done in search of alternative strategies for N_2 fixation to NH_3 , including electrocatalytic ^{6,7}, photocatalytic ⁸, biological ⁹, and plasma-based ¹⁰ methods, but none of these methods have yet been able to rival the overall performance of HB process with regard to the cost efficiency, scalability and selectivity of NH_3 production ^{6,11,12}.

In parallel, it is also of paramount interest to explore alternative molecular mechanisms of fixing N_2 that would obviate the production of NH_3 and thus alleviate the current dependence of society on NH_3 ^{3,13-15}. The global production and utilization of NH_3 are associated with a great number of critical issues, including its severe environmental implications, toxicity, flammability, explosion hazards, corrosiveness, difficulties of transportation and storage, etc, which are increasingly at odds with the paradigm of sustainable development ³. In fact, the prodigious amounts of NH_3 utilized on Earth at present time are to a larger degree dictated by the scarcity of alternative routes of N_2

fixation rather than by the intrinsic usability of NH_3 . Up to date, several catalytic systems have been demonstrated to have a potential of activating the super-strong $\text{N}\equiv\text{N}$ triple-bond, however their practical applications are yet to be explored¹⁵⁻¹⁷. N_2 fixation into NH_3 and NO_y (NO , NO_2 , NO_3 , HNO_3 , HNO_2 , *etc*) has been reported in several plasma-based methods^{10,12,18}. However, NO_y are toxic to the environment. Also, the production of NH_3 and NO_y in plasma-based methods currently comes at the cost of N_2 dissociation/burning and therefore poor chemical selectivity and high energy costs^{10,12}.

Recent studies indicate that the $\text{N}\equiv\text{N}$ bond can be weakened by accepting electrons from the bonding orbitals of N_2 to the antibonding orbitals and/or donating electrons, which would make its functionalization feasible¹⁹. The weakening of $\text{N}\equiv\text{N}$ bond could be further promoted through the excitation of N_2 into its triplet state, *e.g.*, by electronic or collisional activation^{20,21}. Recently, we have discovered that abundant radical cations of water clusters, especially in the dimer form, $(\text{H}_2\text{O})_2^{+\bullet}$, can be produced by depositing suitable amounts of energy into the pure water vapor at atmospheric pressure²². The as-prepared water radical cations showed the high reactivity toward a wide range of volatile molecules, such as benzene, acetone, ethyl acetate and dimethyl disulphide, revealing rich chemistry with the ionic and radical characters²²⁻²⁵. Here we discovered that, owing to its distinct 2c-3e configuration, $(\text{H}_2\text{O})_2^{+\bullet}$ can specifically activate N_2 via the formation of $\text{HONH-HNOH}^{+\bullet}$ intermediate to selectively disproportionate it into hydroxylamine (NH_2OH) and nitroxyl (HNO) products under mild ambient conditions and with no catalyst involved.

Results and discussion

In our first experiment, water plasma was generated by discharge of water/argon vapor mixture (Supplementary Fig. 1a). The major ionic species observed by real-time mass spectrometry detection included protonated water clusters, $(\text{H}_2\text{O})_2\text{H}^+$ (m/z 37) and $(\text{H}_2\text{O})_3\text{H}^+$ (m/z 55), as well as abundant water dimer radical cation, $(\text{H}_2\text{O})_2^{+\bullet}$ (m/z 36) (Supplementary Fig. 1b), in agreement with previous reports²²⁻²⁷. Remarkably, when N_2 was introduced to intersect with the water plasma (Fig. 1a) or when the carrier gas (Ar) in the ion source was replaced by N_2 , abundant ions of m/z 32 and m/z 33 and m/z 64 were additionally observed (Fig. 1b). We tentatively assigned these signals to HNOH^+ (m/z 32), $\text{NH}_2\text{OH}^{+\bullet}$ (m/z 33) and $\text{HONH-HNOH}^{+\bullet}$ (m/z 64), respectively. We speculated that these new ionic species could be derived through the reaction between $(\text{H}_2\text{O})_2^{+\bullet}$ and N_2 . To verify this assumption, $(\text{H}_2\text{O})_2^{+\bullet}$ ions (m/z 36) were isolated and activated in the ion trap by RF field ($\sim 100 \text{ V}_{\text{p-p}}$) in the presence of neutral N_2 gas, which was directly introduced into the ion trap. As the result, the product signals were unambiguously observed at m/z 18 (elimination of H_2O from $(\text{H}_2\text{O})_2^{+\bullet}$), m/z 19 (elimination of $\bullet\text{OH}$ from $(\text{H}_2\text{O})_2^{+\bullet}$), m/z 33 ($\text{NH}_2\text{OH}^{+\bullet}$), m/z 51 ($\text{NH}_2\text{OH}^{+\bullet}$ plus H_2O), m/z 55 ($(\text{H}_2\text{O})_3\text{H}^+$) and m/z 64 ($\text{HONH-HNOH}^{+\bullet}$) (Fig. 1c). Curiously, the signal of HNOH^+ abundantly produced upon the interaction between water plasma and N_2 (m/z 32 in Fig. 1b) was almost undetectable when $(\text{H}_2\text{O})_2^{+\bullet}$ was activated in the ion trap (Fig. 1c), probably because the HNO was initially created as neutral species. During the interaction between water plasma and N_2 , neutral HNO could be easily protonated by other ionic species such as $(\text{H}_2\text{O})_2\text{H}^+$ (m/z 37) to give the protonated signal at m/z 32 (Fig. 1b), whereas when produced in the ion trap neutral HNO would be instantly pumped out of the ion trap (maintained at high vacuum of 10^{-5} Torr).

The signal at m/z 64 was assigned to HONH-HNOH⁺ intermediate produced during the reaction between N₂ and (H₂O)₂⁺ inside the ion trap. The chemical assignment of the m/z 64 signal to HONH-HNOH⁺ was supported by collision-induced dissociation (CID) data (Fig. 1d), showing the characteristic fragment at m/z 33 corresponding to the elimination of HNO, accompanied by lower-intensity fragments at m/z 46 and m/z 47 (also discerned in the spectra Fig. 1b, c), corresponding to the elimination of H₂O and [•]OH (the dissociation path shown in Supplementary Fig. 1c), respectively. These chemical assignments were further supported by experiments with isotopic substituents (Fig. 1e, Supplementary Fig. 1d, e). When H₂O in our experiments was replaced by deuterated water, D₂O, the abundant signals at m/z 33, m/z 34 and m/z 35 (Supplementary Fig. 1d) were observed, indicating the formation of HNOD⁺, DNOD⁺/NH₂OD⁺, and NHDOD⁺, respectively. Similarly, when N₂ was replaced by ¹⁵N₂, the signals at m/z 33 and m/z 34 were detected (Fig. 1e), indicating the formation of H¹⁵NOH⁺ and ¹⁵NH₂OH⁺, respectively. Interestingly, the HONH-HNOH⁺-type intermediate was also detected in the experiments with isotopic substitutes: as DOND-DNOD⁺ (m/z 68) for the D₂O experiment (Supplementary Fig. 1d) and as HO¹⁵NH-H¹⁵NOH⁺ (m/z 66) for the ¹⁵N₂ experiment (Fig. 1e), respectively. Note that the intermediates labeled with different isotopes showed the identical fragmentation path (Supplementary Fig. 1e). Further reference experiments carried out in our lab indicated that the observed nitrogen disproportionation occurred specifically as the result of reaction between neutral N₂ and water radical cations: no products could be detected when isolated N₂⁺ was exposed to neutral water vapor in the ion trap (Supplementary Fig. 1f). Therefore, the spectral data

obtained in all the above-mentioned experiments strongly indicate that the observed species correspond to the disproportionation reaction of N_2 with $(\text{H}_2\text{O})_2^{+\cdot}$.

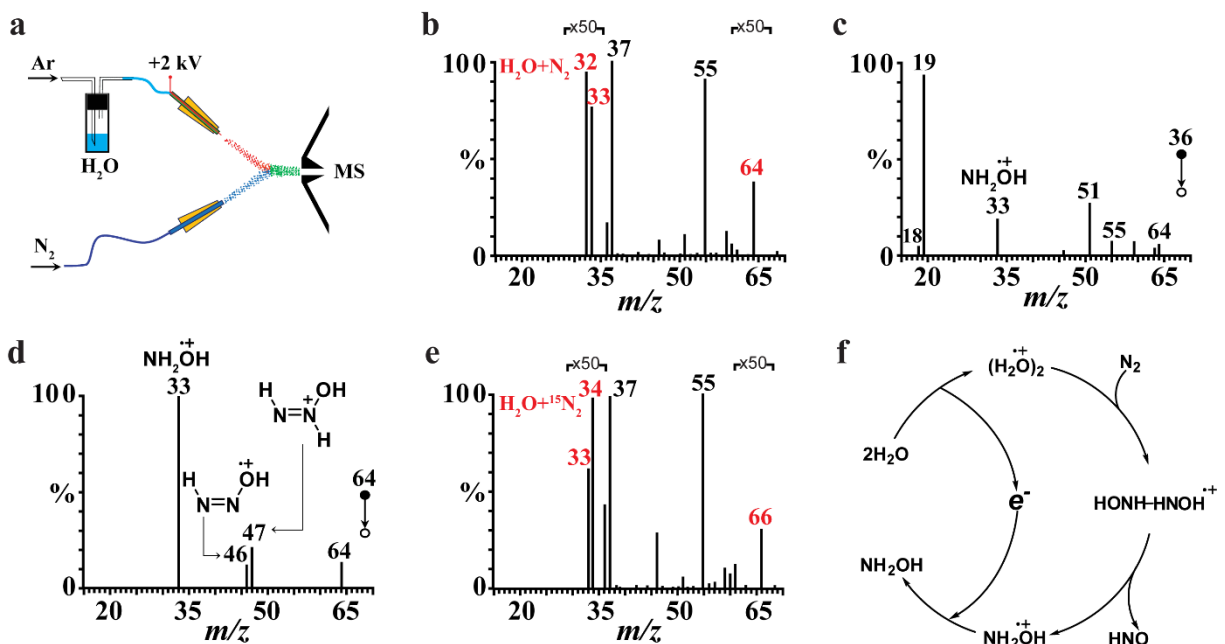


Fig. 1 | Ambient disproportionation reaction of N_2 with water dimer radical cation. (a) Experimental setup to study the interaction of N_2 with water vapor plasma by online mass spectrometry. (b) Mass spectrum of the ionic species. Red-color marks correspond to the products specific to the reaction between water vapor plasma and N_2 . (c) Mass spectrum of ionic products for the gas-phase reaction between N_2 and isolated $(\text{H}_2\text{O})_2^{+\cdot}$ (m/z 36) in the ion trap. (d) Ionic fragments of the reaction intermediate at m/z 64. (e) Mass spectrum of the ionic species observed during the interaction between water vapor plasma and $^{15}\text{N}_2$ ($^{15}\text{N}_2$ gas instead of $^{14}\text{N}_2$ in a). Red-color marks correspond to the products specific to the reaction between water vapor plasma and $^{15}\text{N}_2$. (f) Schematic diagram summarizing a possible mechanism for the reaction of N_2 with $(\text{H}_2\text{O})_2^{+\cdot}$.

Reaction mechanism

Derived from the experimental observations and theoretical calculations, a possible reaction pathway for N_2 disproportionation with $(\text{H}_2\text{O})_2^{+\cdot}$ is proposed as shown in Fig. 1f and Fig. 2. First, neutral H_2O is ionized to form $(\text{H}_2\text{O})_2^{+\cdot}$ species²²⁻²⁵. Our calculations indicate that N_2 disproportionation with $(\text{H}_2\text{O})_2^{+\cdot}$ is thermodynamically not allowed ($\Delta E \approx 4.0$ eV) when N_2

present in its ground singlet ($X^1\Sigma_g^+$) state (Supplementary Fig. 2) but may occur ($\Delta E \approx -3.8$ eV) when N_2 is present in its more active triplet ($A^3\Sigma_u^+$) state, N_2^* (Fig. 2). It is well known that N_2 is effectively transferred from its singlet state to its triplet state through the collisions with electrons (*e.g.*, in N_2 and CO_2 gas lasers), ions or molecules²⁰. It has been shown that, owing to its high molecular symmetry, N_2^* exhibits unique stability and lives for up to 1.3 s²⁸, which allows its involvement in chemical reactions, such as the above-mentioned N_2 disproportionation. In our experiments singlet N_2 could be activated to triplet N_2^* through collisions: with high-energy charged species in the ion source (Fig. 1a, b) or with accelerated $(H_2O)_2^{+\bullet}$ species in the ion trap (Fig. 1c). Our calculations indicate that out of the two co-existing $(H_2O)_2^{+\bullet}$ structures, *i.e.*, hydrogen-bonded $[H_3O^+\cdots OH]$ and two-center-three-electron (2c-3e) $[H_2O\cdots OH_2]^{+22}$, the latter could effectively react with N_2^* (Fig. 2).

The association of $[H_2O\cdots OH_2]^+$ structure with N_2^* occurs due to stabilization of the positive charge jointly by the N_2 and the two H_2O moieties (INT1*, Fig. 2). The INT1* structure is then converted into the excited-state intermediate HONH-HNOH^{+\bullet*} (INT3*, $\Delta E = -1.2$ eV, Fig. 2) by the direct double-proton transfer through TS* structure (Fig. 2). The HONH-HNOH^{+\bullet*} intermediate spontaneously and irreversibly dissociates into neutral HNO and cationic NH_2OH^+ ($\Delta E = -1.5$ eV, Fig. 2). In addition to the dissociation channel, HONH-HNOH^{+\bullet*} could also relax to its ground state, HONH-HNOH⁺ (INT3, $\Delta E = -2.8$ eV, Fig. 2), without dissociation. It is probably through this latter channel that the stable HONH-HNOH⁺ signal is detected in our experiments (m/z 64, Fig. 1). The HONH-HNOH⁺ structure could dissociate into HNO and NH_2OH^+ by collisional activation ($\Delta E = 1.3$ eV, Fig. 2), just as observed in the ion trap experiments (Fig. 1d). The NH_2OH^+ product can be neutralized to NH_2OH by electron transfer from the environment.

Overall, it is clear that N_2 fixation by $(\text{H}_2\text{O})_2^{2+}$ via HONH-HNOH^{2+} intermediate is mechanistically distinct from the earlier described processes of catalytic nitrogen fixation at a heterogeneous surface²⁹, in which nitrogen reduction on metal catalyst usually proceeds via N_2H_x -type intermediates ($0 \leq x \leq 2$). Therefore, this report presents a new mechanism of N_2 fixation.

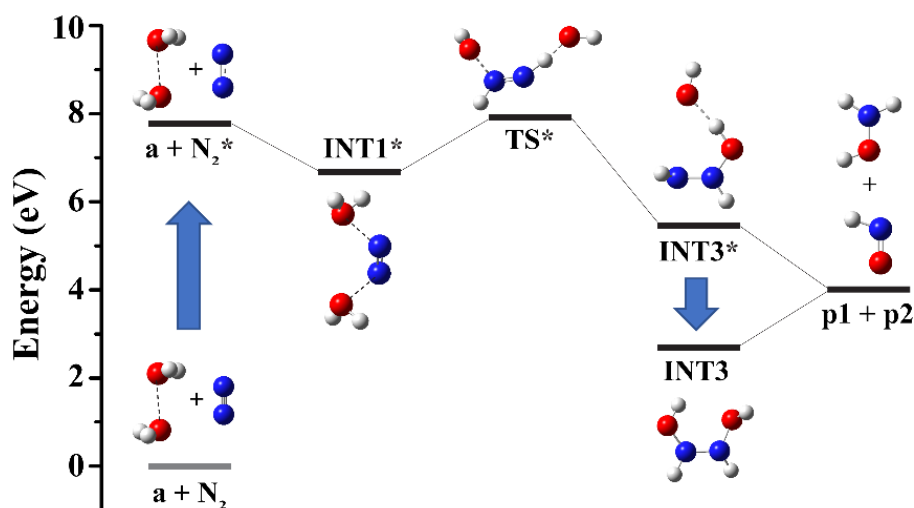


Fig. 2 | The geometries and electronic energies of possible molecular and ionic species involved in the disproportionation reaction $\text{N}_2 + (\text{H}_2\text{O})_2^{2+} \rightarrow \text{NH}_2\text{OH}^{2+} + \text{HNO}$ calculated with B2GP-PLYP density functional. Vertical arrow corresponds to electronic excitation of N_2 . a: $[\text{H}_2\text{O}\cdots\text{OH}_2]^+$. p1: $\text{NH}_2\text{OH}^{2+}$. p2: HNO .

Scale-up reaction

The disproportionation reaction of N_2 with $(\text{H}_2\text{O})_2^{2+}$ was scaled up under ambient conditions using the setup in Fig. 3a, which consisted of an array of 76 needles evenly distributed on a $\sim 3.5 \times 5.5 \text{ cm}^2$ tungsten plate to generate abundant $(\text{H}_2\text{O})_2^{2+}$ and the accessories to collect the NH_2OH and HNO products. We found that NH_2OH was most efficiently collected at the cathode electrode, while HNO was most efficiently collected through the neutral outlet line (Fig. 3a).

These observations further support the conclusion that NH_2OH in the reaction was formed in cationic form while HNO was formed in neutral form.

Under the optimized experimental conditions (Supplementary Fig. 3), the production of $18.5\mu\text{M}$ NH_2OH and $17.7\mu\text{M}$ HNO products could be achieved within just 10 min, as quantified by standard spectrophotometric methods (Supplementary Fig. 4). The collected NH_2OH was reacted with an optical probe 8-quinolinol to form indooxine, which was quantified by UV-Vis spectroscopy³⁰. The signal intensity showed clear correlation with the time of the reaction between N_2 and $(\text{H}_2\text{O})_2^{+}$ (Fig. 3b). The formation of indooxine due to the reaction between NH_2OH and 8-quinolinol was further confirmed by tandem MS experiments through the comparison with indooxine standard (Supplementary Fig. 5a). The formation of NH_2OH product due to the disproportionation reaction between N_2 and $(\text{H}_2\text{O})_2^{+}$ was further validated by infrared (Fig. 3c) and Raman (Fig. 3d) spectroscopy of the collected samples.

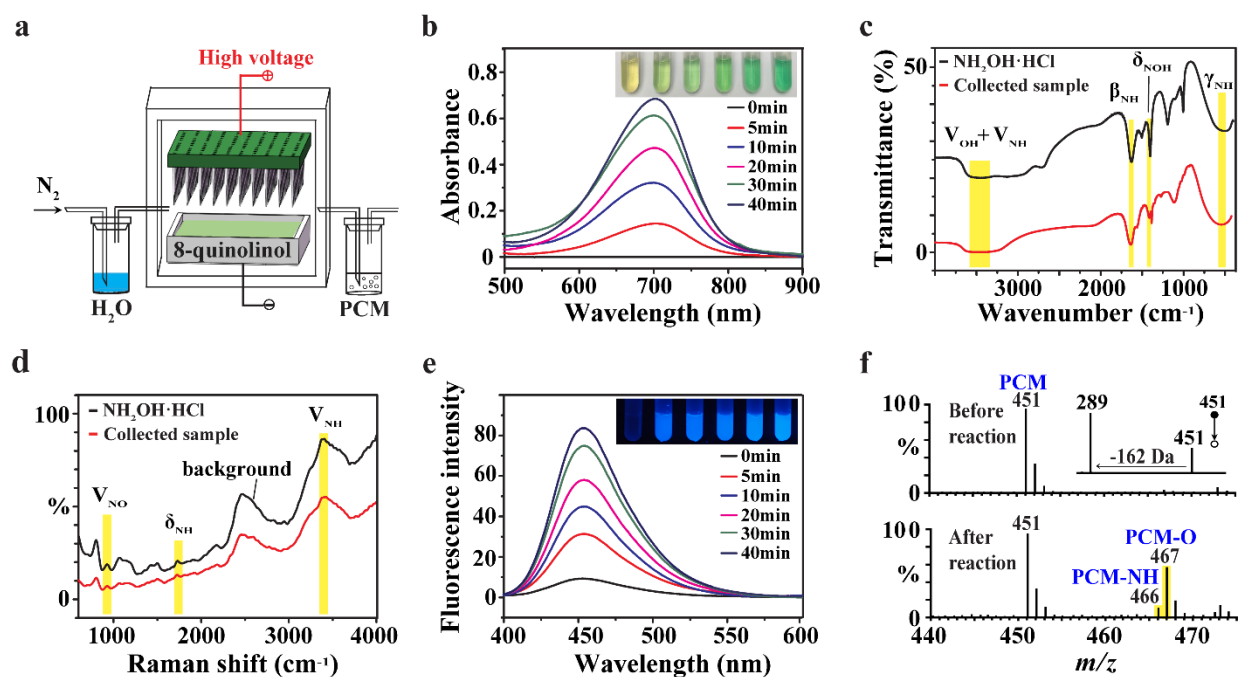


Fig. 3 | Products of ambient disproportionation reaction of N_2 with $(\text{H}_2\text{O})_2^{+}$ characterized by spectral methods. (a) Schematic illustration of the reaction assembly for scale-up reaction

and the collection of reaction products. **(b)** UV-Vis spectra of indooxine formed through the online reaction of the collected NH_2OH with 8-quinolinol probe at different times of the reaction between N_2 and $(\text{H}_2\text{O})_2^{+\bullet}$. **(c)** Infrared spectra of the collected sample (red) and $\text{NH}_2\text{OH}\cdot\text{HCl}$ standard (black). **(d)** Raman spectra of the collected sample (red) and $\text{NH}_2\text{OH}\cdot\text{HCl}$ standard (black). **(e)** Fluorescence spectra of 7-hydroxycoumarin formed through the online reaction of the collected HNO with PCM probe at different times of the reaction between N_2 and $(\text{H}_2\text{O})_2^{+\bullet}$. **(f)** Mass spectra of PCM solution before and after collection of the reaction mixture, showing the formation of PCM aza-ylide (PCM-NH) and PCM oxide (PCM-O) due to the reaction between PCM and HNO. The inset figure shows the tandem mass spectrum of protonated PCM at m/z 451.

Similarly, the collected HNO was reacted with a coumarin-based fluorescent probe PCM to form 7-hydroxycoumarin. The 7-hydroxycoumarin was quantified by fluorescence spectroscopy. The signal intensity showed clear correlation with the time of the reaction between N_2 and $(\text{H}_2\text{O})_2^{+\bullet}$ (Fig. 3e). The occurrence of the reaction between PCM and the HNO product was further confirmed by the detection of other products of the reaction between PCM and HNO: the PCM aza-ylide and PCM oxide (Fig. 3f, Supplementary Fig. 5b), which were in good agreement with the literature data³¹. Note that the preparation and characterization of PCM is described in the Supplementary Fig. 5c, d.

Reference experiments performed using the scaled-up setup shown in Fig. 3a when N_2 was replaced by Ar showed the total absence of characteristic NH_2OH and HNO signals in the collected samples, thus indicating that the NH_2OH and HNO products were generated specifically due to the reaction of $(\text{H}_2\text{O})_2^{+\bullet}$ with N_2 (Supplementary Fig. 6). Therefore, the reference measurements and the mass spectrometry, vibrational spectroscopy and optical spectroscopy data altogether provide unambiguous proofs for the formation of NH_2OH and HNO in the disproportionation reaction between N_2 and water radical cations $(\text{H}_2\text{O})_2^{+\bullet}$.

Application of the reaction products

Note that the both products of the disproportionation reaction between N_2 and $(\text{H}_2\text{O})_2^{+\bullet}$ are highly valuable chemicals. For example, NH_2OH is widely used as an important chemical raw

material, *e.g.* to prepare oximes ³², anilines ³³, amides ³⁴, and sulfonamides ³⁵, as well as energetic fuel for space rockets ³⁶. Further, using a low-cost homemade setup powered by a 1.5 V solar cell battery (Supplementary Fig. 7a) in our laboratory, we were able to easily reduce the prepared NH_2OH into NH_3 (Fig. 4a) with the conversion rate of almost 100% within ca. 30 min (Fig. 4b). The simplicity of the experimental assembly suggests that the disproportionation reaction between N_2 and $(\text{H}_2\text{O})_2^{+\bullet}$ could probably serve the agricultural fields as tiny onsite ammonia plants, which could be powered by solar cells ³⁷.

The other reaction product, HNO (as the active ingredient of medicine such as Angeli's salt (AS) ³⁸, is a currently expensive material for medical and biology utilities ^{39,40}, particularly for biological targets of thiols and metalloproteins in fighting cancer ⁴¹. Further, here we also showed that the HNO product of the reaction between N_2 and $(\text{H}_2\text{O})_2^{+\bullet}$ could be used to directly convert cysteine into cystine (Fig. 4c) with the conversion rate of almost 100% within ca. 60 min (Fig. 4d) under the conditions tested, suggesting that HNO could be used for the specific chemical modification of thiols in proteins, which is consistent with previous report of authentic AS ³⁸. These data further validate the formation of NH_2OH and HNO during the reaction between N_2 and $(\text{H}_2\text{O})_2^{+\bullet}$ and demonstrate the potential applications of these products.

Importantly, HNO is known for its cardioprotective and neuroprotective effects ^{39,40}. In addition, HNO is resistant to superoxide scavenging and tolerance development ⁴². Here we investigated whether the HNO product of disproportionation reaction could be used for protection against neurotoxicity. Fig. 4e shows the effect of HNO concentration levels on the viability of HT22 cells. The results indicate that the application of HNO in the range from 0.008 μM to 1 μM poses no cytotoxic effect on the HT22 cells and promotes their proliferation. The EC_{50} and IC_{50} were estimated as 0.016 μM and 18.12 μM , respectively (Supplementary Fig. 8a,

b). The viability of HT22 cells was greatly reduced when exposed to exogenous source of free radicals, H₂O₂ at 200 μM (~50%, P < 0.01 vs. the control group) (Fig. 4f, Supplementary Fig. 8c, d). Remarkably, HT22 cells incubated with HNO displayed significantly higher resistance to the H₂O₂-induced damage, with maximum protection at 0.25 μM concentration of HNO (79%, P < 0.01 vs. the H₂O₂ group) (Fig. 4f). The results of our cell viability assay indicate that the HNO product could be used to protect HT22 cells against H₂O₂-induced damage. As the research continues in this field, it is likely that further novel properties, endogenous actions and therapeutic applications of HNO will be discovered.

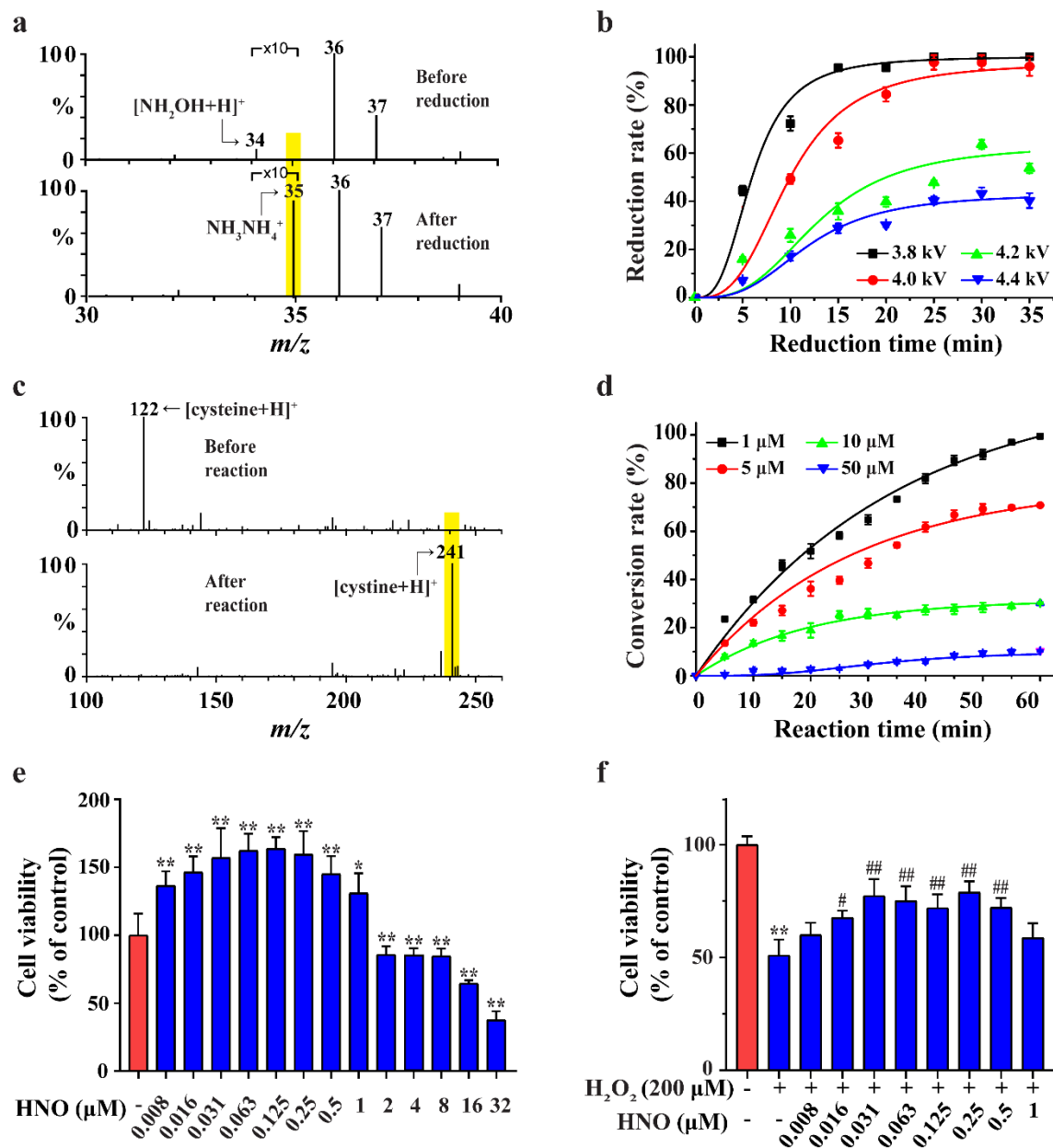


Fig. 4 | Further validation and application of the NH_2OH and HNO products of N_2 disproportionation with $(H_2O)_2^{+\bullet}$. (a) Electrolytic reduction of the collected NH_2OH product (corresponding signal at m/z 34) into NH_3 (corresponding signal at m/z 35) confirmed by MS detection. The signals at m/z 36 and m/z 37 correspond to $(H_2O)_2^{+\bullet}$ and $H^+(H_2O)_2$. (b) The kinetics of electrolytic reduction of NH_2OH collected at different discharge voltages into NH_3 determined using the indophenol blue method (45) (see Supplementary Fig. 7). (c) The conversion of cysteine (corresponding signal at m/z 122) into cystine (corresponding signal at m/z 241) via the reaction of cysteine with the collected HNO product of the disproportionation reaction of N_2 confirmed by MS detection. (d) The kinetics of cysteine conversion into cystine via the reaction with the collected HNO product ($\sim 25 \mu M$; collection time 30 min) at different cysteine concentrations. (e) Effects of different concentration levels of HNO alone on HT22 cell viability. (f) HT22 cells were pretreated with different concentration levels of HNO for 24 h and

incubated with or without H₂O₂ (200 μM) for 1 h. Cell viability as determined with CCK-8 assay. **P*<0.05 and ***P*<0.01 versus control, #*P*<0.05 and ###*P*<0.01 versus model.

Characteristics of the N₂ disproportionation reaction

Using the total plate area ($\sim 3.5 \times 5.5 \text{ cm}^2$) as the active area of the 76-pin device (Fig. 3a), we estimated the Faradic efficiency (FE) $\approx 64\%$ with the yield $\approx 1.14 \mu\text{g cm}^{-2} \text{ h}^{-1}$ for NH₂OH and the FE $\approx 20\%$ with the yield $\approx 0.37 \mu\text{g cm}^{-2} \text{ h}^{-1}$ for HNO (optimized in Supplementary Fig. 9). Note that the maximum yields calculated based only on the total effective surface area of 76 needle tips were $5.10 \times 10^3 \mu\text{g cm}^{-2} \text{ h}^{-1}$ for NH₂OH and $1.53 \times 10^3 \mu\text{g cm}^{-2} \text{ h}^{-1}$ for HNO, respectively, since only the tip surface of the needles were activated for the N₂ disproportionation reaction (see detailed footnotes in Supplementary Table 1). The lower yield and FE for HNO is probably caused by its higher reactivity, resulting in the partial conversion of HNO by H₂O and other chemicals in the collecting solution. Compared to the majority of previously reported approaches for nitrogen reduction under mild conditions (Supplementary Table 1)⁴³, including plasma methods (Supplementary Table 2), our method provides reasonably high efficiency and yield. Other key merits of our method include: 1) mild conditions; total avoidance of toxic reagents and by-products; low cost; easy implementation; scalability; 2) low energy consumption, high efficiency and high-value products: according to the current market, the potential value about 1.5 \$ of NH₂OH and 7310 \$ of HNO (as derived from the AS application) were produced by 1 kWh of electricity (≤ 0.2 \$); 3) no chemical catalyst needed; 4) high atom economy: the oxidation of one nitrogen atom of N₂ to HNO coupled with the simultaneous reduction of the other nitrogen atom of N₂ to NH₂OH.

In summary, we have demonstrated that the atmospheric N₂ can be disproportionately fixed by (H₂O)₂⁺⁺ under ambient conditions into economically valuable NH₂OH and HNO, presenting

an alternative to the current necessity of fixing N_2 into NH_3 . The combination of the essential N, O and H atoms in the obtained products considerably increases variability of possible chemistries as compared to NH_3 ^{33,44}. The experimental and theoretical studies indicate that triplet-state N_2 is activated by $(H_2O)_2^{+*}$ to form intermediate $HONH-HNOH^{+*}$, which is further decomposed to form NH_2OH^{+*} and HNO. The mechanism of N_2 fixation by the 2c-3e $(H_2O)_2^{+*}$ structure through the excited-state double-proton transfer is principally different from the previously proposed methods. The design ideas in this work could motivate more research efforts to further explore the potential of distinct $(H_2O)_2^{+*}$ chemistry and open new possibilities for green nitrogen fixation.

References

1. Yeung, L. Y. et al. Extreme enrichment in atmospheric $^{15}N^{15}N$. *Sci. Adv.* **3**, 6741 (2017).
2. Legare, M. A. et al. Nitrogen fixation and reduction at boron. *Science* **359**, 896-899 (2018).
3. Erisman, J. W., Sutton, M. A., Galloway, J., Klimont, Z. & Winiwarter, W. How a century of ammonia synthesis changed the world. *Nat. Geosci.* **1**, 636-639 (2008).
4. Chen, J. G. et al. Beyond fossil fuel-driven nitrogen transformations. *Science* **360**, aar6611 (2018).
5. Tanabe, Y. & Nishibayashi, Y. Comprehensive insights into synthetic nitrogen fixation assisted by molecular catalysts under ambient or mild conditions. *Chem. Soc. Rev.* **50**, 5201-5242 (2021).
6. Li, J. et al. Fundamentals and advances in emerging crystalline porous materials for photocatalytic and electrocatalytic nitrogen fixation. *ACS Appl. Energy Mater.* **5**, 9241-9265 (2022).
7. Fang, Y. et al. Graphdiyne interface engineering: Highly active and selective ammonia synthesis. *Angew. Chem. Int. Ed.* **59**, 13021-13027 (2020).
8. Vu, M.-H., Sakar, M., Hassanzadeh-Tabrizi, S. A. & Do, T.-O. Photo(electro)catalytic nitrogen fixation: Problems and possibilities. *Adv. Mater. Interfaces* **6**, 1900091 (2019).
9. Soumare, A. et al. Exploiting biological nitrogen fixation: A route towards a sustainable agriculture. *Plants* **9**, 1011 (2020).
10. Winter, L. R. & Chen, J. G. N_2 fixation by plasma-activated processes. *Joule* **5**, 300-315 (2021).
11. Martín, A. J., Shinagawa, T. & Pérez-Ramírez, J. Electrocatalytic reduction of nitrogen: From Haber-Bosch to ammonia artificial leaf. *Chem* **5**, 263-283 (2019).
12. Huang, Z., Xiao, A., Liu, D., Lu, X. & Ostrikov, K. Plasma-water-based nitrogen fixation: Status, mechanisms, and opportunities. *Plasma Process. Polym.* **19**, 2100198 (2022).
13. Erisman, J. W. et al. Consequences of human modification of the global nitrogen cycle. *Philos. T. R. Soc. B* **368**, 20130116 (2013).
14. Wang, Q., Guan, Y., Guo, J. & Chen, P. Hydrides mediate nitrogen fixation. *Cell Rep. Phys. Sci.* **3**, 100779 (2022).

15. McWilliams, S. F. et al. Coupling dinitrogen and hydrocarbons through aryl migration. *Nature* **584**, 221-226 (2020).
16. Knobloch, D. J., Lobkovsky, E. & Chirik, P. J. Dinitrogen cleavage and functionalization by carbon monoxide promoted by a hafnium complex. *Nat. Chem.* **2**, 30-35 (2010).
17. MacLeod, K. C. et al. Alkali-controlled C–H cleavage or N–C bond formation by N₂-derived iron nitrides and imides. *J. Am. Chem. Soc.* **138**, 11185-11191 (2016).
18. Pattyn, C. et al. Disproportionation of nitrogen induced by DC plasma-driven electrolysis in a nitrogen atmosphere. *Green Chem.* **24**, 7100-7112 (2022).
19. Wang, Q., Guo, J. & Chen, P. The impact of alkali and alkaline earth metals on green ammonia synthesis. *Chem* **7**, 3203-3220 (2021).
20. Kirkici, H., Bruno, D., Preiss, J. & Schaefer, G. Charge-transfer collisions between He₂⁺ ions and N₂: Branching ratio into vibrational states. *J. Appl. Phys.* **67**, 6041-6044 (1990).
21. Ristić, M. M., Aoneas, M. M., Vojnović, M. M. & Poparić, G. B. Excitation of electronic states of N₂ in radio-frequency electric field by electron impact. *Plasma Chem. Plasma Process.* **37**, 1431-1443 (2017).
22. Wang, M. et al. Abundant production of reactive water radical cations under ambient conditions. *CCS Chem.* **3**, 3559-3566 (2022).
23. Zhang, X., Ren, X., Zhong, Y., Chingin, K. & Chen, H. Rapid and sensitive detection of acetone in exhaled breath through the ambient reaction with water radical cations. *Analyst* **146**, 5037-5044 (2021).
24. Mi, D. et al. Generation of phenol and molecular hydrogen through catalyst-free C-H activation of benzene by water radical cations. *J. Am. Soc. Mass Spectrom.* **33**, 68-73 (2022).
25. Zhang, X. et al. Mass spectrometry distinguishing C=C location and cis/trans isomers: a strategy initiated by water radical cations. *Anal. Chim. Acta* **1139**, 146-154 (2020).
26. Xing, D. et al. Capture of hydroxyl radicals by hydronium cations in water microdroplets. *Angew. Chem. Int. Ed.* **61**, e202207587 (2022).
27. Qiu, L., Morato, N. M., Huang, K.-H. & Cooks, R. G. Spontaneous water radical cation oxidation at double bonds in microdroplets. *Front. Chem.* **10**, 903774 (2022).
28. Sharpe, S. W. & Johnson, P. M. Triplet Rydberg states in molecular nitrogen. *J. Chem. Phys.* **85**, 4943-4948 (1986).
29. Yao, Y., Wang, H., Yuan, X.-z., Li, H. & Shao, M. Electrochemical nitrogen reduction reaction on ruthenium. *ACS Energy Lett.* **4**, 1336-1341 (2019).
30. Frear, D. S. & Burrell, R. C. Spectrophotometric method for determining hydroxylamine reductase activity in higher plants. *Anal. Chem.* **27**, 1664-1665 (1955).
31. Mao, G.-J. et al. A highly sensitive and reductant-resistant fluorescent probe for nitroxyl in aqueous solution and serum. *Chem. Commun.* **50**, 5790-5792 (2014).
32. Dal Pozzo, L., Fornasari, G. & Monti, T. TS-1, catalytic mechanism in cyclohexanone oxime production. *Catal. Commun.* **3**, 369-375 (2002).
33. Zhu, L. F. et al. Sodium metavanadate catalyzed one-step amination of benzene to aniline with hydroxylamine. *J. Catal.* **245**, 446-455 (2007).

34. Deng, X., Zhou, G., Tian, J. & Srinivasan, R. Chemoselective amide-forming ligation between acylsilanes and hydroxylamines under aqueous conditions. *Angew. Chem. Int. Ed.* **60**, 7024-7029 (2021).
35. Zhu, H., Shen, Y., Deng, Q., Huang, C. & Tu, T. One-pot bimetallic Pd/Cu-catalyzed synthesis of sulfonamides from boronic acids, DABSO and O-benzoyl hydroxylamines. *Chem. Asian J.* **12**, 706-712 (2017).
36. Zhao, F. et al. A simple and efficient approach for preparation of hydroxylamine sulfate from the acid-catalyzed hydrolysis reaction of cyclohexanone oxime. *Chem. Eng. J.* **272**, 102-107 (2015).
37. Du, Z., Denkenberger, D. & Pearce, J. M. Solar photovoltaic powered on-site ammonia production for nitrogen fertilization. *Sol. Energy* **122**, 562-568 (2015).
38. Walter, M. R. et al. Synthesis of $\text{Co}^{\text{II}}\text{-NO}^-$ complexes and their reactivity as a source of nitroxyl. *J. Am. Chem. Soc.* **138**, 12459-12471 (2016).
39. Tian, Y., Paolocci, N. & Gao, W. D. Nitroxyl, a new generation of positive inotropic agent for heart failure. *Engineering* **1**, 401-404 (2015).
40. Sun, H.-J. et al. Role of nitroxyl (HNO) in cardiovascular system: From biochemistry to pharmacology. *Pharmacol. Res.* **159**, 104961 (2020).
41. Shoman, E. M. & Aly, M. O. Nitroxyl (HNO): a possible strategy for fighting cancer. *Curr. Top. Med. Chem.* **16**, 2464-2470 (2016).
42. Irvine, J. C. et al. Nitroxyl (HNO): the Cinderella of the nitric oxide story. *Trends Pharmacol. Sci.* **29**, 601-608 (2008).
43. Xue, X. et al. Review on photocatalytic and electrocatalytic artificial nitrogen fixation for ammonia synthesis at mild conditions: advances, challenges and perspectives. *Nano Res.* **12**, 1229-1249 (2019).
44. An, X.-D. & Yu, S. Direct synthesis of nitriles from aldehydes using an O-benzoyl hydroxylamine (BHA) as the nitrogen source. *Org. Lett.* **17**, 5064-5067 (2015).
45. Wang, X. et al. Atomically dispersed Au_1 catalyst towards efficient electrochemical synthesis of ammonia. *Sci. Bull.* **63**, 1246-1253 (2018).
46. Zhu, D., Zhang, L., Ruther, R. E. & Hamers, R. J. Photo-illuminated diamond as a solid-state source of solvated electrons in water for nitrogen reduction. *Nat. Mater.* **12**, 836-841 (2013).
47. Frisch, M. J. et al. Gaussian 16. *Revision A.03*, **Gaussian, Inc.**, Wallingford, CT (2016).
48. Pan, P.-R., Lin, Y.-S., Tsai, M.-K., Kuo, J.-L. & Chai, J.-D. Assessment of density functional approximations for the hemibonded structure of the water dimer radical cation. *Phys. Chem. Chem. Phys.* **14**, 10705-10712 (2012).
49. Huber, K. P. & Herzberg, G. in *Molecular Spectra and Molecular Structure: IV. Constants of Diatomic Molecules* (eds K. P. Huber & G. Herzberg) 8-689 (Springer US, 1979).

Methods

Chemicals and Material. Hydroxylamine (NH₂OH), 8-quinolinol and 2-(diphenylphosphino) benzoic acid were purchased from Shanghai Sun Chemical Technology Co., Ltd (China), with a purity > 99%. D₂O was purchased from Cambridge Isotope Laboratories, Inc. (Andover, MA, USA). Authentic Angeli's salt (AS) used in fluorescence quantification experiments was purchased from Cayman Chemical and stored at -20 °C. Ultra-purity N₂ (> 99.99%), ultra-purity helium (> 99.99%), ultra-purity argon (> 99.99%) and ultra-purity ¹⁵N₂ (> 99.99%) were obtained from Jiangxi Guoteng Gas Co. Ltd (Nanchang, China). Water used in all experiments was purified by a Milli-Q system (Millipore, USA).

Foetal bovine serum (FBS) was purchased from Zhejiang Sorfa Life Science Co., Ltd. (Zhejiang, China). Dulbecco's modified eagle's medium (DMEM), Trypsin-EDTA solution and PBS were obtained from Solarbio Life Science Co., Ltd. (Beijing, China). H₂O₂ (30%) was purchased from Xilong Scientific Co., Ltd. (Guangdong, China). The CCK8 assay kit was obtained from Biosharp Life Sciences Co., Ltd. (Anhui, China). Microplate reader was purchased from Gene Company Limited (Hong Kong SAR, China). CO₂ incubator was obtained from SANYO (Osaka, Japan). Inverted microscope was purchased from Leica (Germany). Superclean bench was from Suzhou Purification Co., Ltd. (Shanghai, China).

The coumarin-based fluorescent probe PCM was synthesized in our lab according to the method reported by Tan *et al* with modification³¹. In detail, 2-(diphenylphosphino) benzoic acid (306 mg, 1 mmol) was dissolved in 50 mL of anhydrous CH₂Cl₂ under inert atmosphere. Then, 4-(dimethylamino) pyridine (6.1 mg, 0.05 mmol) and 1-ethyl-3-(3-dimethylaminopropyl) carbodiimide hydrochloride (191.7 mg, 1mmol) were added, and the reaction mixture was stirred at room temperature for 30 min. 7-hydroxycoumarin (194.6 mg, 1.2 mmol) was then added, and

the resulting mixture was stirred at room temperature. The reaction mixture was concentrated under reduced pressure. The residue was purified by the silica gel chromatography (EtOAc/petroleum ether =1:2, v/v) to yield PCM product as a faint yellow solid. ^1H NMR (CDCl_3 , 500MHz) δ (ppm): 8.278-8.245 (m, 1H), 7.681-7.657 (d, $J = 9.6$ Hz, 1H), 7.502-7.474 (m, 2H), 7.440-7.418 (m, 1H), 7.377-7.277 (m, 10H), 7.022-6.989 (m, 1H), 6.930-6.902 (m, 2H), 6.396-6.372 (d, $J = 9.6$ Hz, 1H). MS (ESI) m/z 451.0 $[\text{M}+\text{H}]^+$ (Fig. 3f).

Reaction between N_2 and $(\text{H}_2\text{O})_2^{+\bullet}$ with real-time MS detection. Experimental setup to study the products of the reaction between N_2 and $(\text{H}_2\text{O})_2^{+\bullet}$ in real time is shown in Fig. 1a. In order to produce $(\text{H}_2\text{O})_2^{+\bullet}$, neutral Ar gas was bubbled through liquid H_2O at a flow rate of 10~100 mL min^{-1} , and the produced $\text{H}_2\text{O}/\text{Ar}$ vapor was guided to the home-made ambient corona discharge ion source through Teflon tubing (ID 0.75 mm). To build the ion source, a sharp discharge needle (stainless steel; OD 150 μm ; end curvature radius ~ 30 μm) was coaxially inserted into a fused silica capillary (ID 0.25 mm, OD 0.40 mm) and was fixed coaxially with a union tee and silica ferrule. The back end of the tee was connected to the $\text{H}_2\text{O}/\text{Ar}$ line. The distance from the inlet of the mass spectrometer capillary to the tip of the ion source was 20 mm. The high voltage of +2.0 kV was applied to the stainless-steel needle in order to generate ambient corona discharge. A flow of neutral N_2 (100 mL min^{-1}) was introduced through a separate channel to interact with the produced $(\text{H}_2\text{O})_2^{+\bullet}$. In a reference experiment, N_2 was replaced by Ar (Supplementary Fig. 1a).

Scale-up reaction between N_2 and $(\text{H}_2\text{O})_2^{+\bullet}$. The experimental setup for the scaled-up disproportionation reaction between N_2 and $(\text{H}_2\text{O})_2^{+\bullet}$ with the collection of reaction products is presented in Fig. 3a. High-purity N_2 controlled by mass flow controller was bubbled through liquid H_2O and was then transferred through the discharge reactor in quartz enclosure toward the

outlet tubing connected with a collection bottle. The reactor consisted of a discharge array of 76 tungsten needles under direct current voltage (anode) and a flat grounded electrode (cathode). The distance between the tips of two adjacent needles was evenly set as 0.5 cm. Cationic reaction product (NH_2OH^+) was collected by an indium tin oxide (ITO) coated glass bottle filled with 8-quinolinol probe solution (6 mL), which was placed on the top of the cathode. Neutral reaction product (HNO) was pumped out through the outlet line into the bottle filled with PCM probe solution (2 mL) (Fig. 3a). The amount of electric charge neutralized on the cathode plate was determined by an electrochemical workstation (Shanghai Chenhua Instrument Co., Lt, CHI660E).

Mass spectrometry settings. Mass spectrometry (MS) detection was carried out using an LTQ-XL ion trap mass spectrometer (LTQ-XL, Thermo Scientific, San Jose, CA, USA). The temperature of the ion transfer capillary was 150 °C. The capillary voltage was 1.0 V. The tube lens voltage was 30.0 V. The pressure of ion trap was 1×10^{-5} torr. High-purity helium (99.99%) was used as the collision gas. The collision-induced dissociation (CID)-MS experiments were performed by applying excitation alternating current voltage to the end caps of the ion trap to induce collisions of the isolated ions. The CID-MS spectra were obtained by activation of the precursor ions at the normalized collision energy varied from 0% to 50%. Ion detection was done in the positive ion mode. Other LTQ-XL parameters were automatically optimized by the system.

Quantification of NH_2OH by UV-Vis spectroscopy. The concentration of collected NH_2OH was determined by the 8-quinolinol color test method with modification³⁰. In detail, 1.2 mL phosphate buffer (0.05 M, pH 6.8), 0.24 mL trichloroacetic acid solution and 1.2 mL sodium carbonate solution (1.0 M) were mixed in a tube. Then 1.2 mL ethanol solution of 8-quinolinol

(10 mg mL⁻¹) was added. Finally, pure water was added into the tube to bring the solution volume to 6 mL. Thus prepared 6 mL reagent solution was placed on top of the cathode plate. The N₂ disproportionation reaction was then started. The ultraviolet-visible (UV-Vis) absorption spectra of the solution were measured at different reaction times (0, 5, 10, 20, 30, 40 min) on a spectrophotometer (SP-1920, Shanghai Spectrum Instrument Co., Ltd). The formation of indooxine due to the reaction between NH₂OH and 8-quinolinol was evident by the characteristic absorbance band with the maximum at 705 nm. For calibration, UV-Vis spectra were collected for a series of blank (zero time of disproportionation reaction) reagent solutions spiked with different concentrations of NH₂OH (0.01 mM, 0.05 mM, 0.1 mM, 0.2 mM, 0.25 mM), showing good linear correlation of indooxine absorbance with NH₂OH concentration by three independent measurements (Supplementary Fig. 4a, b). Blank UV-Vis measurements were also done when no NH₂OH was added.

Characterization of NH₂OH by infrared and Raman spectroscopy. The collected samples and NH₂OH•HCl standard were analyzed on a Thermo Nicolet iS5 Fourier transform infrared spectrograph. In detail, KBr samples were powdered and spread evenly on top of the cathode plate (Fig. 3a). The N₂ disproportionation reaction was then run over 24 h. The sample collected on the cathode plate was analyzed by infrared spectroscopy. NH₂OH•HCl sample was measured for control.

The collected samples and NH₂OH•HCl standard were also analyzed by Via RM2000 laser Raman spectroscopy (Renishaw company, United Kingdom) with 10 s integration time in the spectral range of 400–4000 cm⁻¹. CW laser irradiation at the wavelength of 532 nm was focused through a 50X objective to excite the samples. Deionized water was placed on top of the cathode plate (Fig. 3a). The N₂ disproportionation reaction was run over 48 h. The product collected on

the cathode plate was analyzed by Raman spectroscopy. The authentic $\text{NH}_2\text{OH}\cdot\text{HCl}$ solution was analyzed for control.

Quantification of HNO by fluorescence spectroscopy. The amount of collected HNO was estimated by the method reported by Tan et al.³¹. PCM probe was freshly dissolved in DMF to obtain 1 mM stock solution, which was diluted to 10 μM with 100 mM PBS buffer (pH 7.4). The prepared PCM solutions (10 μM , total volume = 2 mL) were connected to the reactor outlet line as shown in Fig. 3a for different periods of reaction time at room temperature. The fluorescence of 7-hydroxycoumarin formed through the reaction of HNO with the PCM probe was excited at 370 nm and was measured at 450 nm. Fluorescence from the blank PCM (10 μM) solution (not reacted with HNO) was measured as control. The yields of HNO were calculated from a standard curve using AS as HNO source. A stock solution of AS (2 $\mu\text{M mL}^{-1}$) was prepared in 1 M NaOH solution and stored at -20°C . 20 μL AS standard solutions with different concentrations (0.01 μM , 0.25 μM , 1 μM , 2 μM , 5 μM) were separately added into 10 μM PCM solutions to bring the volume to 2 mL. Then, fluorescence spectra were recorded. The fitting curve showed good linearity of fluorescence intensity at 450 nm with HNO concentration by three independent measurements (Supplementary Fig. 4c, d).

Experiments on HT22 cells treated with HNO product. In the present experiments, we established H_2O_2 -induced oxidative stress models in HT22 cells to investigate whether HNO has anti-oxidative stress and neuroprotective effects. HNO was generated using the disproportionation reaction of N_2 with $(\text{H}_2\text{O})_2^{+*}$ under ambient conditions. HT22 cells were purchased from Procell Life Science & Technology Co., Ltd. and cultured in DMEM supplemented with 10% (v/v) FBS and 1% penicillin/streptomycin at 37°C with the atmosphere of 5% CO_2 . To induce cell damage, H_2O_2 was added to the culture for 1 hour.

The HT22 cells were seeded in 96-well plates (0.8×10^5 cells/well) and incubated with different concentrations of HNO for 24 h followed by H₂O₂ treatment. Cell viability was examined by the Cell Counting Kit-8 assay kit (Dojindo, Tokyo, Japan). The absorbance of the samples was measured at 450 nm by microplate reader. The cell survival ratio was expressed as the percentage of the control.

All of the statistical analyses were performed by the SPSS 21.0 software. All of the data are expressed as the mean \pm SD. Comparison between the two groups was assessed with an unpaired t-test, while comparison among several groups was evaluated using one-way ANOVA. The p-value < 0.05 was considered statistically significant.

Calculation of the Faradaic efficiency and yield. For the experiment setup shown in Fig. 3a, the yields of NH₂OH and HNO were calculated using the following equations reported in earlier literature ⁴⁵:

$$\text{Yield}_{\text{NH}_2\text{OH}} = (C_{\text{NH}_2\text{OH}} \times V_{\text{NH}_2\text{OH}} \times M_{\text{NH}_2\text{OH}}) / (t \times S) \quad (1)$$

$$\text{Yield}_{\text{HNO}} = (C_{\text{HNO}} \times V_{\text{HNO}} \times M_{\text{HNO}}) / (t \times S) \quad (2)$$

where V is the volume of absorption solution ($V_{\text{NH}_2\text{OH}} = 6$ mL; $V_{\text{HNO}} = 2$ mL), t is the reaction time (10 min), C is the concentration of the collected product over 10 min (*e.g.*, at 4.2 kV: $C_{\text{NH}_2\text{OH}} = 18.5$ μM and $C_{\text{HNO}} = 17.7$ μM , determined using calibration curves in Supplementary Fig. 4), M is the molar mass of a collected product ($M_{\text{NH}_2\text{OH}} = 33$ g mol⁻¹; $M_{\text{HNO}} = 31$ g mol⁻¹), S is the total effective surface area to conduct the reaction. The S value is measured by microscope (detailed in footnotes in Table S1).

The FE for N₂ reduction was determined as the amount of electric charge used for the generation of NH₂OH divided by the total charge passed through the cathode electrode during

reaction. The FE for N₂ oxidation was determined as the amount of electric charge used for the generation of HNO divided by the total charge passed through the electrodes during reaction. Assuming that one electron is needed to produce one HNO molecule and one NH₂OH molecule (Fig. 1f), the FE value was calculated as described by Wang *et al*⁴⁵:

$$FE = (n \times F \times C \times V) / Q \quad (3)$$

where n is the number of electrons transferred in the reaction ($n = 1$ in our case); F is the Faraday's constant ($F = 96485.33 \text{ C mol}^{-1}$); C is the concentration of the collected NH₂OH or HNO; V is the volume of absorption solution to collect NH₂OH or HNO; and Q denotes the total charge passed through the cathode electrode during reaction (0.0168 C over 10 min reaction at 4.2 kV).

Reduction of NH₂OH to ammonia. To quantify the amount of NH₂OH collected during N₂ disproportionation reaction, the NH₂OH product of N₂ disproportionation reaction was collected into an ITO coated glass bottle filled with the solution of 8-quinolinol probe (Fig. 3a) for 30 min. The concentration of indooxine produced through the reaction between NH₂OH and 8-quinolinol was quantified by UV-Vis experiments (Supplementary Fig. 4a), and the concentration of collected NH₂OH was derived accordingly. Then, under the exactly identical conditions, the NH₂OH product of N₂ disproportionation reaction was collected into an ITO coated glass bottle filled with deionized water (without 8-quinolinol). The solution containing NH₂OH was transferred into a cell for electrochemical reduction, which was powered by a 1.5 V solar cell battery (Supplementary Fig. 7). The positive and negative electrodes (diameter 0.5 mm) connected to the 1.5 V battery were immersed into the solution to a depth of 1 cm for 35 min. The formation of NH₃ was confirmed by MS analysis (Fig. 4a). The concentration of generated ammonia was spectrophotometrically determined using the indophenol blue method⁴⁶. In detail,

a 1 mL of the solution from the electrochemical reduction bottle was transferred into a 15 mL centrifuge tube. Then, 9 mL of 0.005 mol L⁻¹ sulfuric acid aqueous solution, 0.5 mL of 50 g L⁻¹ salicylic acid solution containing 50 g L⁻¹ sodium citrate and 2 mol L⁻¹ NaOH solution, 0.1 mL of 0.05 mol L⁻¹ NaClO and 0.1 mL of 10g L⁻¹ Na₂[Fe(NO)(CN)₅]•2H₂O were added into the tube and mixed. After 1 h, the absorption spectrum was measured using UV-Vis spectrophotometer (Supplementary Fig. 7). The formation of indophenol blue product was determined by measuring the absorbance at 705 nm. The calibration of the method was achieved using ammonium chloride solutions of known concentration as standards. The concentration of NH₃ was derived from the calibration curve (Supplementary Fig. 7).

Reaction of HNO with cysteine. The reaction of HNO with cysteine was investigated using the setup shown in Fig. 3a. The experiment was done under the same conditions as in Fig. 3a, with the exception that the PCM probe solution in the collection bottle was replaced with cysteine solution at different concentrations (1-50 μM). Cystine produced by the reaction between HNO and non-reacted cysteine were detected by mass spectrometry analysis (Fig. 4c).

Theoretical calculations. Theoretical calculations were performed using the Gaussian 16 electronic structure programs⁴⁷. The geometries of reactants, intermediates and products were optimized at dispersion-corrected density functional theory level (DFT-D) with closed- and open-shell virtual orbital-dependent functional as first introduced by Grimme (B2PLYP, commonly referred to as B2-PLYP), which uses more than half of exact exchange energy. We used the modification of this functional by Martin (B2GP-PLYP) that is expected to be capable of 2 kcal mol⁻¹ quality thermochemistry and to be robust toward nondynamical electron correlation. To estimate the practical uncertainty of our electronic energy differences, we also

used the revised version of DSD-PBEP86 functional with Grimme's BJD3 empirical dispersion correction: relative energy differences ≈ 0.12 eV were observed during this comparison.

Complex Dunning's correlation consistent basis sets of triple and quadruple quality were used to build molecular orbitals: Truhlar's may-cc-pVTZ set was applied for a preliminary optimization, while fully augmented aug-cc-pVQZ basis set was used for the final results. Force constants and the resulting vibrational frequencies were obtained at "very tightly" converged geometries with RMS force threshold of 10^{-6} Hartree Bohr⁻¹. Pruned "ultra-fine" grids with 99 radial shells and 590 angular points per shell were used for all calculations. Vibrational frequencies of all the key species were calculated at the same level of theory to obtain their Gibbs free energies at 300 K.

Highly parameterized Minnesota global hybrid functional from Truhlar with 54% of HF exchange (M06-2X) and τ -dependent meta-gradient-corrected (meta-GGA) functional of Tao, Perdew, Staroverov, and Scuseria (TPSS, commonly referred to as TPSS/TPSS) were used to further estimate the uncertainty of quantum chemical calculations⁴⁸. Modification of PBE0 density functional by setting its exact exchange energy to 7.5% was also tested. Transition state energy was estimated from the combination of B2PLYP and M06-2X data.

Our choice of virtual orbital-dependent functionals was determined by a comparison with available experimental data in literature⁴⁹. Dinitrogen (N₂) represents an example of complicated electronic system with large static electron correlation (also known as "strongly correlated system"²⁸). Therefore, popular DFT functionals (B3LYP, PBE0, wB97X, etc.) are not applicable to N₂, while B2PLYP and its analogs are able to precisely reproduce the experimental data. For example, the bond length and harmonic frequency (ω_e) of the ground-state singlet N₂ ($X^1\Sigma_g^+$) calculated by B2PLYP are 109.78 pm and 2346 cm⁻¹, accordingly. These numbers are highly

consistent with the experimental values of 109.77 pm and 2359 cm⁻¹. For comparison, the same results for B3LYP functional are less accurate: 109.01 pm and 2448 cm⁻¹. The dispersion-corrected functional from Head-Gordon (wB97XD) is even less accurate: 108.72 pm and 2490 cm⁻¹. The same conclusion holds for the triplet N₂ (A ³Σ_u⁺ and B ³Π_g states) as well as for the ground doublet state of N₂⁺ (X ²Σ_g⁺).

Acknowledgments:

The authors acknowledge Dr. Lili Sun for preliminary calculations. The authors also thank Ms. Xuejiao Chen and Mr. Yuan Zhong for their help in designing the MS experiments. The authors are particularly grateful for the proof reading of the manuscript by Prof. Yinquan Wang. The work was supported by National Natural Science Foundation of China (No.21520102007, 22104014).

Author Contributions H.C. independently developed the idea of the research, supervised the project and prepared the manuscript. X.Z. (*i.e.*, the 1st author) collected the MS data, interpreted the MS data, and co-wrote the manuscript draft. K.C., X.Z. (*i.e.*, the 1st author), W.Z., R.B. and H.C. edited the manuscript. L.H., J.W., W.Z and H.C. designed and conducted the HT22 cells experiments, collected and analyzed the data. X.Z. (*i.e.*, the 8th author), J.L., W.Y., R.S., K.H., S.F. and X.Z. (*i.e.*, the 1st author) collected the UV-Vis, fluorescence spectroscopy, IR, Raman and NMR data. R.B. conducted all the calculations.

Competing interests: The authors have no competing interests.

Data and materials availability: All data are available in the main text or the supplementary materials.